NATIONAL AERONAUTICS AND SPACE ADMINISTRATION

Technical Report 32-1084

A Comparison of Some Predicted and Measured Variables for a Full-Scale Surveyor Drop Test

J. A. Garba

Approved by:

M. E. Alper

M. E. Alper, *Manager*
Applied Mechanics Section

JET PROPULSION LABORATORY
CALIFORNIA INSTITUTE OF TECHNOLOGY
PASADENA, CALIFORNIA

March 1, 1967

TECHNICAL REPORT 32-1084

Prepared Under Contract No. NAS 7-100
National Aeronautics & Space Administration

Acknowledgment

The author is indebted to T. E. Lang, of JPL, for his constant encouragement and to Mrs. C. Level and Mrs. M. Blount, both of JPL, for their help in the data reduction. Grateful acknowledgment is also made to the Hughes Aircraft Company, Culver City, California, for the use of the Figures and data in this Report.

Contents

Contents (contd)

Tables

Figures

Contents (contd)

Figures (contd)

Abstract

This Report describes the correlation between the predicted and measured dynamic behavior for a full-size *Surveyor* drop test. The investigation includes a detailed examination of the test uncertainties encountered in a full-scale stability drop of a three-legged vehicle and the effect of such uncertainties on the correlation between experimental and theoretical results. Time histories of the pertinent variables are presented and discussed.

A Comparison of Some Predicted and Measured Variables for a Full-Scale *Surveyor* Drop Test

I. Introduction

In the development of lunar and planetary soft-landing vehicles, such as *Surveyor* or the *Lunar Module*, landing stability is of great importance. Vehicle stability is usually investigated as a function of the landing velocities, vehicle orientation, surface slope, and the coefficient of friction. Some of these variables are bounded by system considerations, others are functions of the local environment which is not known.

The investigation of the stability of a soft-landing vehicle requires a detailed study of the spacecraft motion. Due to the complexity of the landing systems employing various energy absorption mechanisms, such as hydraulic shock absorbers, crushable footpads, and body blocks, a sophisticated mathematical model is required. To obtain the time-motion history of the spacecraft, a numerical integration routine must be employed. Care must be taken to insure that the integration routine gives good results. Since the tools used to establish vehicle stability are rather complex, it is imperative to confirm the theoretical predictions by experiment. It is the purpose of this Report to present and discuss theoretical and experimental correlation for one planar drop of the *Surveyor* spacecraft. The test results are discussed in the light of uncertainties in the test parameters and their effect on the computer predictions. Variations in the coefficient of sliding friction, the gravity force, and the touchdown velocities are studied in the range of observed uncertainties. Predicted and measured time histories of the pitch angle, pitch rate, shock-absorber forces, leg deflections, and leg lower-strut moments are examined in detail.

The test data were obtained from *Surveyor* full-size drop tests conducted by the Hughes Aircraft Company. The tests were conducted during April 1966 at the high-temperature structural test laboratory of the Hughes Aircraft Company in Culver City, California. The test vehicle consisted of the dynamic model (S-15) of the *Surveyor* spacecraft. The test program is described in Ref. 1.

The *Surveyor* touchdown stability program, developed for JPL by the Bendix Products Aerospace Division, was used to obtain the theoretical predictions.

II. Computer Simulation

During the developmental phase of a complex lunar landing system such as the one employed by the *Surveyor* spacecraft (see Fig. 1), it is essential to develop analytical tools for the optimization and evaluation of the landing-gear design. The analytical approach is favored over the purely experimental approach since parameters affecting the landing-gear design can be studied more expeditiously and economically.

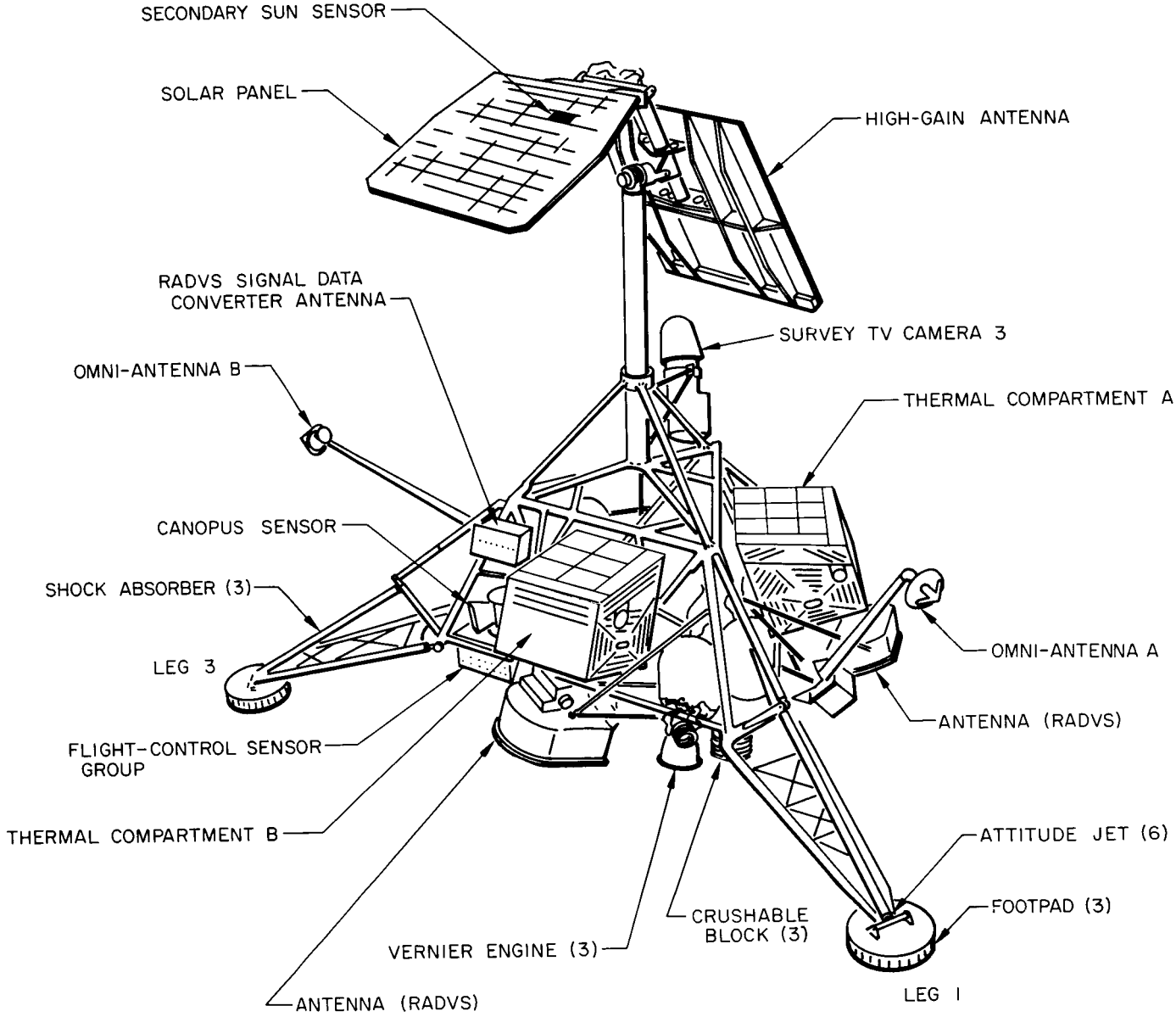

Fig. 1. *Surveyor* spacecraft in touchdown configuration

A digital computer program has been developed by the Bendix Products Aerospace Division under contract to JPL for the analysis of the touchdown dynamics of a three-legged vehicle. The development of this program originated from the requirement for the generation of stability boundaries for the *Surveyor* spacecraft landing on a hard surface as a function of the following independent touchdown parameters: linear velocity of the vehicle center of gravity (c.g.), angular rates about vehicle fixed axes, vehicle attitude, lunar slope, and the coefficient of friction between the spacecraft and the lunar surface.

A. Mathematical Model

In the digital computer program, the *Surveyor* spacecraft is represented by the main body, which is considered to be rigid, and the landing system. The landing system, a schematic of which is shown in Fig. 2, is further broken down into the three articulating inverted tripod legs, three landing feet (footpads), and three crushable body blocks.

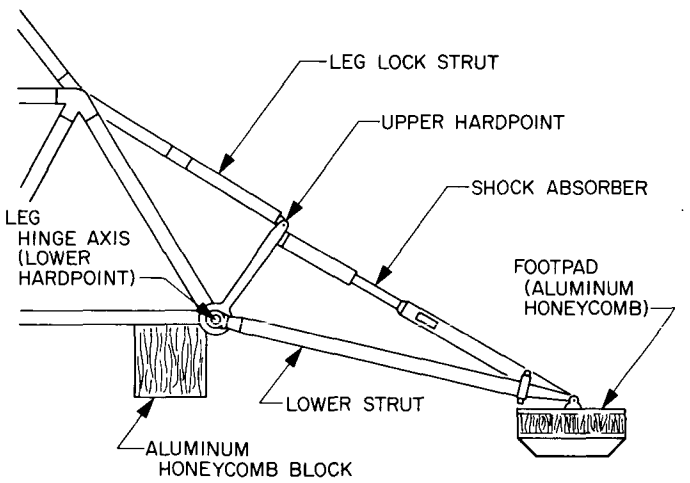

Fig. 2. Landing-gear schematic

Two of the members of the inverted tripod landing leg form the rigid lower strut. This lower strut is mathematically treated as a single rigid link rotating about the leg hinge axis and connecting the lower hardpoint to the footpad pivot. This link is capable of carrying a moment in the plane of the lower strut.

The third member of the inverted tripod leg contains the hydraulic shock absorber. The shock absorber carries an axial load only and connects the upper hardpoint on the main body to the footpad pivot. Mathematically, the shock absorber is described as exhibiting a force opposing velocity and displacement as a nonlinear function of displacement.

The landing feet, free to pivot about an axis in the plane of the lower strut, exhibit force-opposing displacement. The force is a function of the angle of the applied load, the contact area, and the crushing displacement. Due to the footpad geometry, the crushing force vs displacement is not constant.

The crushable blocks are mathematically similar to the footpads. Their crushing force, however, is a function of the contact area only.

Detailed force characteristics for the shock absorbers, crushable body blocks, and the footpads are given in Appendix A.

In formulating the equations of motion for the complete system, the following degrees-of-freedom are considered: the three translations and three rotations of the main body, one angular position of each of the legs with respect to the main body, and one angular position of each of the footpads with respect to the legs. The external forces and torques acting on the spacecraft are considered to arise from the ground reaction, friction forces, and from gravity.

The above formulation leads to 12 nonlinear second-order differential equations. The solution of these equations over an incremental time interval establishes a new geometrical configuration of the vehicle which in turn determines new forcing functions for the next integration step.

B. Integration Routine

The integration routine used in solving the differential equations of motion is a variable-interval, error-checking fourth-order Runge-Kutta integration procedure with a built-in correction for the estimated fifth-order truncation error.

Using this method, the program will first select an initial integration interval, then will perform three integrations, once over the entire interval and twice over two half intervals. By comparing the difference of the two results with their respective estimated truncation errors, the time interval is either halved and the process repeated, or the consecutive integration time interval is

increased in proportion to the ratio of allowable errors to incurred errors.

This integration scheme not only controls the incurred truncation error, but it also allows the integration time interval to be increased at times when the forcing functions are varying slowly.

The allowable errors are specified, based on program usage experience. For a particular configuration the allowable errors are chosen, such that reducing the allowable errors further would not increase the confidence in the answers.

A detailed derivation of the integration routine, as well as a discussion on the selection of the allowable errors, is contained in Ref. 2 ("Final Report on *Surveyor* Lunar Touchdown Stability Study").

C. Options

The primary objective of the program is to establish the stability or instability of the spacecraft for a particular landing condition. Stability is defined as the capability of the spacecraft to remain in an upright position throughout the touchdown maneuver. This is accomplished as part of the standard output. Several other output options, as described below, are also available.

The additional output options describe the detailed dynamic behavior of the vehicle. The following dependent variables can be computed by the program: variables describing the complete time history of motion of the center of gravity (c.g.) of the spacecraft, minimum clearance between the spaceframe and the ground, and all pertinent forces in the landing-gear system as functions of time. Furthermore, the program can compute a running total of the energy dissipated and stored in each of the energy-absorbing mechanisms of the landing-gear system.

One option of the program was specifically included for the analysis of flight touchdown data. In addition to the standard input describing the spacecraft geometry, inertial properties, and initial conditions, this option also accepts the impact times of the three footpads. Utilizing these impact times, the program calculates the effective slope on which the spacecraft landed and the orientation of the vehicle and its velocity vector with respect to this slope at the time of touchdown. This information can then be used, in connection with telemetry data, to attempt a complete analytical simulation of an actual lunar landing.

D. Coordinate Systems and Symbols

Three coordinate systems are used to describe the vehicle position in space:

1. The basic inertial coordinate system is called the *ground coordinate system* (X, Y, Z) shown in Fig. 3. In this coordinate system, the Z axis is aligned with the gravity vector, positive downward, the Y axis is in the direction of maximum slope, and the X axis completes the right-hand orthogonal triad.

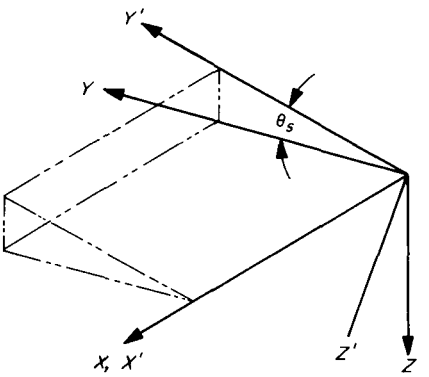

Fig. 3. Ground and surface coordinate systems

2. Figure 3 also shows an additional inertial system (X', Y', Z'). This *surface coordinate system* differs from the ground coordinates only by a rotation θ_s about the X axis. In *surface coordinates*, the X' and Y' axes lie in the plane of the surface, and the Z' axis is normal to the surface, positive downward.

3. The *vehicle coordinate system* (x, y, z), shown in Fig. 4, has its origin at the vehicle c.g. and moves with the vehicle. The z axis is positive downward along the vehicle centerline, the y axis is positive in the direction of Leg Set No. 1, and the x axis completes the right-hand orthogonal triad.

The vehicle coordinate axes are related to the ground coordinate system by the rotations: ψ (pitch), ϕ (yaw), and Ξ (roll). Any angular orientation of the vehicle system with respect to the ground system can be obtained by imagining the vehicle to be aligned with a coordinate system parallel to the ground system and then rotating the vehicle by ψ about the body-fixed x-axis, ϕ about the body-fixed y axis, and finally Ξ about the body-fixed z axis to the desired position.

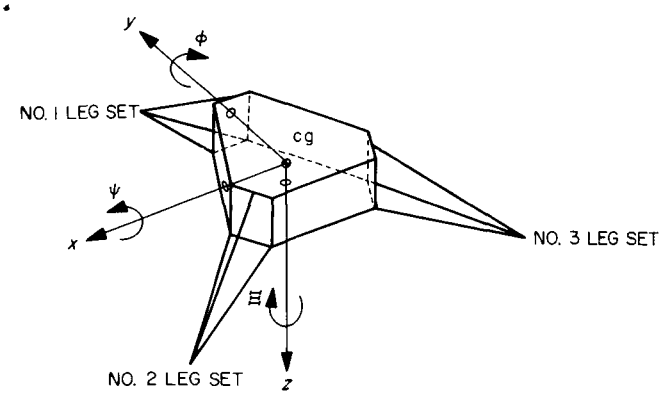

Fig. 4. Vehicle coordinate system

The origin of the ground coordinate system coincides with the c.g. of the vehicle at initial touchdown, $t = 0$.

The pertinent nomenclature is as follows:

g acceleration of gravity, ft/sec/sec

F_i force in the i^{th} shock absorber, lb

I_{xx}, I_{yy}, I_{zz} vehicle centroidal moments of inertia, slug-ft^2

I_{xy}, I_{xz}, I_{yz} vehicle centroidal products of inertia, slug-ft^2

M vehicle mass, slugs

v_x, v_y, v_z velocity components of the vehicle c.g. at touchdown in vehicle coordinates, ft/sec

V_x, V_y, V_z velocity components of the vehicle c.g. at touchdown in ground coordinates, ft/sec

V_H velocity component of the vehicle c.g. at touchdown in the horizontal plane, $V_H = \sqrt{V_x^2 + V_y^2}$, ft/sec

V_v velocity component of the vehicle c.g. at touchdown parallel to the gravity vector, $V_v = V_z$, ft/sec

ΔCG distance from the spacecraft c.g. to the plane defined by the three lower hard-points, ft

θ_s ground slope, deg

μ_B sliding coefficient of friction between the crushable body blocks and the ground, dimensionless

μ_f sliding coefficient of friction between the footpads and the ground, dimensionless

Ψ_0, ϕ_0, Ξ_0 angles defining the vehicle position with respect to the ground coordinate system at touchdown, deg

$\omega_x, \omega_y, \omega_z$ angular rates about vehicle axes, deg/sec

A complete list of variables is given in Ref. 2.

III. Test Description

A. Test Vehicle

A full-size test vehicle, shown in Fig. 5, was employed in the drop test. The test spacecraft consisted of a flight-type spaceframe ballasted to simulate the rigid-body properties of the *Surveyor*. No attempt was made to simulate the elastic characteristics of the main spacecraft body. The landing-gear system consisted of flight-type shock absorbers, aluminum honeycomb crushable footpads, and aluminum honeycomb crushable body blocks (blocks are not shown in Fig. 5). Thus, the test vehicle provided an elastically accurate model of the landing-gear system.

The inertial properties of the test vehicle were as follows:

$$M = 19.2 \text{ slugs}$$

$$I_{xx} = I_{yy} = 134 \text{ slug-ft}^2; \; I_{zz} = 173 \text{ slug-ft}^2$$

$$I_{xy} = I_{xz} = I_{yz} = 0$$

$$\Delta CG = 1.49 \text{ ft}$$

All inertia terms are centroidal. A comparison of the above inertial properties to those of the *Surveyor I* flight spacecraft shows that the test vehicle was 3% lighter than the flight spacecraft, approximately 3% low on I_{xx}, and ΔCG was high by 1 in. All of these deviations of the test vehicle from the flight spacecraft tend to make the test vehicle less stable than the flight spacecraft would be.

B. Test Setup

To obtain the desired vertical and horizontal velocity at the time of touchdown, the test vehicle was suspended from a four-bar linkage pendulum as shown in Fig. 6. The length of the pendulum arms, the horizontal distance the vehicle was pulled back, and the vertical distance the vehicle was allowed to drop, all being variable, determined the touchdown velocities. The platform had a tilt provision for the desired initial attitude. Friction losses in the pendulum were compensated for by calibrating the test setup using a dummy weight. Since

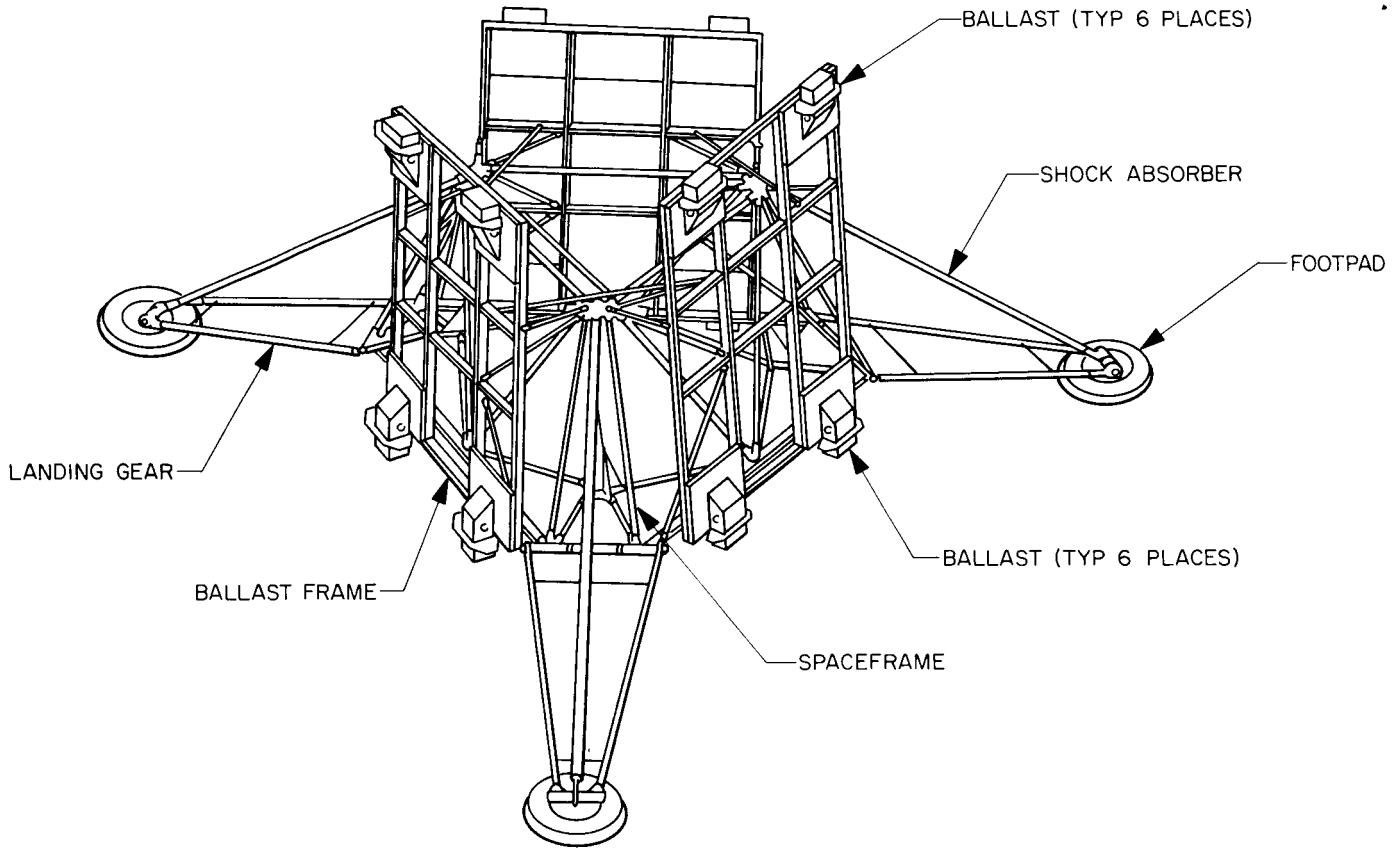

Fig. 5. Test vehicle

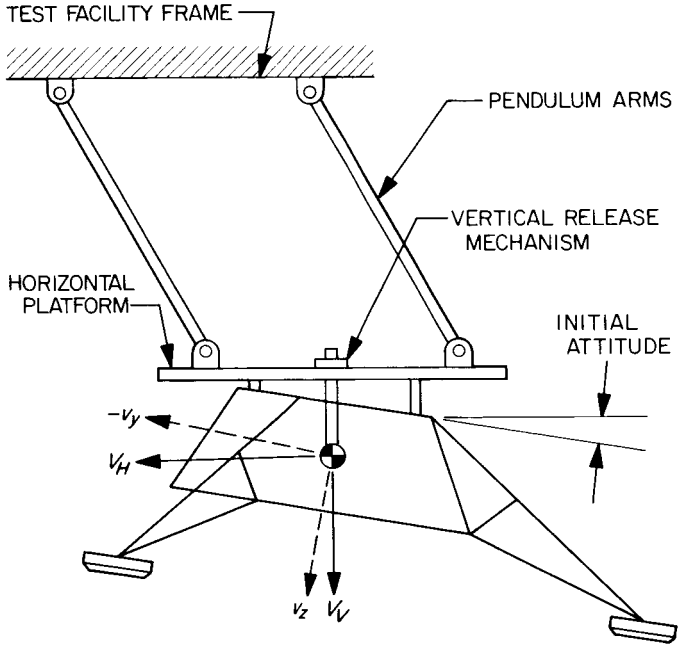

Fig. 6. Schematic of pendulum imparting lateral velocity

the drop test was conducted using a full-size vehicle under Earth gravity, it was required to compensate for 5/6 of the gravity force. Figure 7 shows a schematic of the "anti-gravity" device.

The vehicle was suspended at its c.g. by a continuous cable connecting through a rolling pulley and two stationary pulleys to two air cylinders. The pressure in the air cylinders was kept constant, such that the cable took out 5/6 of the Earth weight of the spacecraft. The reservoir connecting to the air cylinders was large enough to avoid pressure oscillations due to changes in volume. No feedback control system was employed. The weight of the cable and piston rods was minimized to reduce their inertia effect.

In order to minimize the drop height required, the vehicle was first allowed to fall under Earth gravity before the "anti-gravity" force started acting.

The platform onto which the vehicle was dropped was tilted to 15 deg and covered with rubber matting.

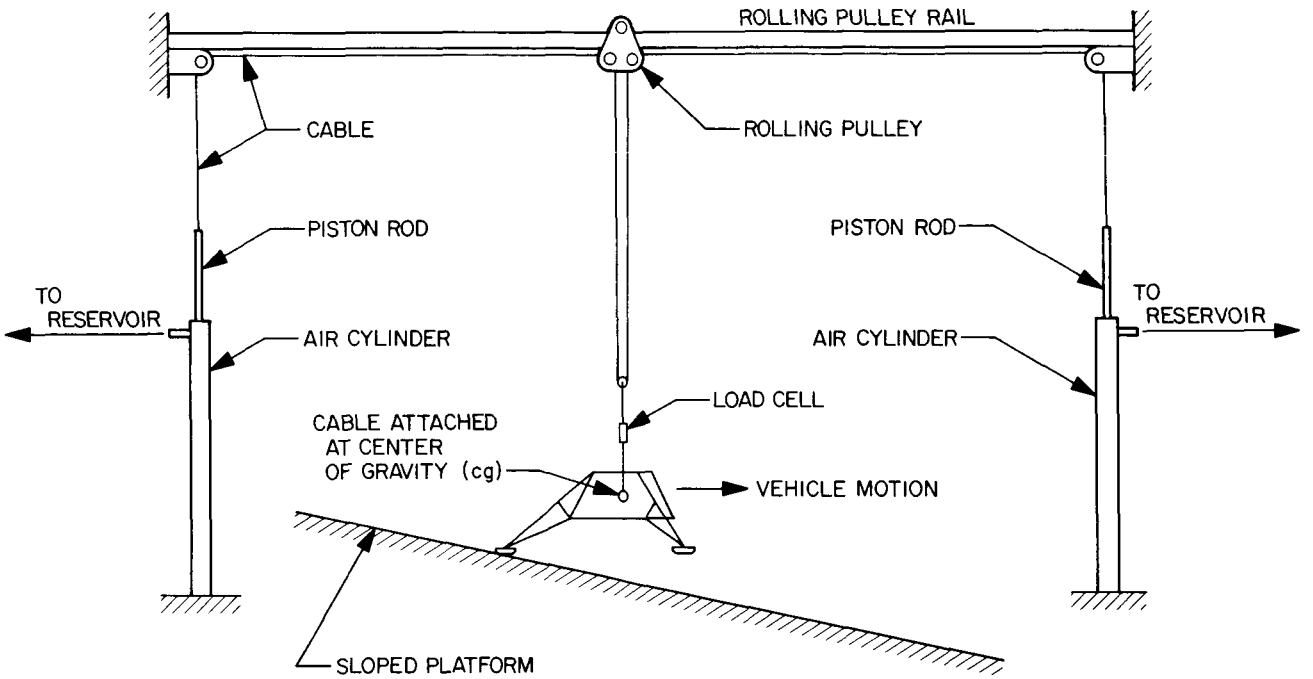

Fig. 7. "Anti-gravity" device schematic

C. Instrumentation

The instrumentation used in the drop-test program is summarized in Table 1. An attempt was made to measure as many time-dependent variables describing the motion and load time histories as practical. There were no transducers available to record the time histories of the c.g. velocity or displacement. All channels were recorded on magnetic tape, and the signals were then reproduced on oscillograph records. The estimated accuracy was arrived at by using the basic system accuracy and adding the resolution of the readout of the oscillograph. It was felt that the accuracies cited in Table 1 are conservative.

Table 1. Instrumentation of S-15 test vehicle

Measurement	Type	No. of channels	Estimated accuracy
Shock absorber forces	Strain gauge	3	±100 lb
Rigid leg forces	Strain gauge	6	±100 lb
Body block forces	Strain gauge	9	±100 lb
Leg deflection	Rotary potentiometer	3	±0.5 deg
Vehicle attitude	Position gyro/ potentiometer	3	±1.0 deg
Vehicle angular rate	Rate gyro/diff. transformer	3	±3.0 deg/sec
Lifting cable force	Load cell	1	±20 lb
Time reference	Oscillator signal	1	±1 cps

D. Test Conditions

The test to be described in this Report is a two-dimensional downhill drop, wherein the vehicle was initially pitched upward such that the angular orientation of the spacecraft at touchdown with respect to the ground coordinate system was given in degrees as

$$\psi_0 = 10; \quad \phi_0 = 0; \quad \Xi_0 = 0$$

Leg No. 1 was trailing.

The nominal touchdown velocities, in vehicle coordinates, were specified in ft/sec as

$$v_x = 0; \quad v_y = -11; \quad v_z = 17$$

The footpads and the platform upon which the vehicle was dropped were covered with rubber matting to produce the desired coefficient of friction.

IV. Test Uncertainties and Their Effect on Computer Predictions

Before comparing theoretical predictions of the *Surveyor* touchdown obtained from a digital computer simulation with actual drop test results, it is important first to examine the accuracy to which some of these variables can be controlled and/or predicted during the test, and second to study the sensitivity of the computer predictions to such variations.

A. Test Uncertainties

In a test setup such as the one described in Section III, there are basically four areas wherein it is difficult to either control or predict certain variables.

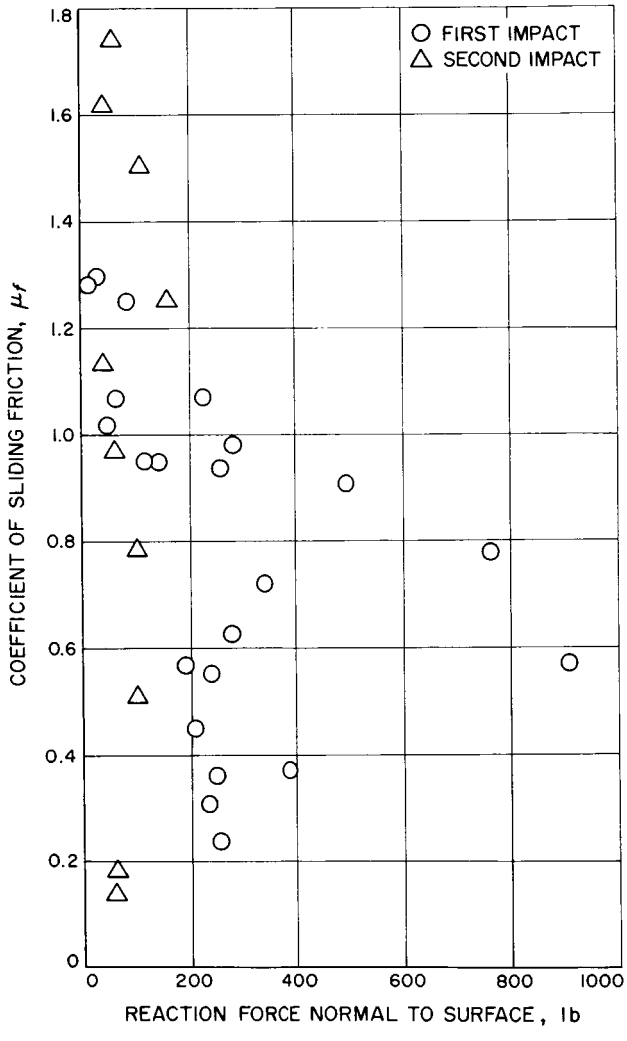

Fig. 8. Coefficient of sliding friction vs reaction force normal to surface; Leg Set No. 1

1. Coefficient of friction. It is expected that the coefficient of sliding friction between the footpads and the surface is a function of:

a. The normal force acting on the footpad

b. The velocity of the footpad

c. The area of contact

d. The footpad attitude.

Every leg set and body block was instrumented, such that the forces on the footpad pivots as well as the body blocks could be defined completely. Furthermore, since the angular position of the lower strut, as well as the vehicle attitude, was known, the landing structure forces could be transferred into surface coordinates to define the coefficient of friction for any time. The forces were assumed to act at the footpad pivot since the position of the footpad was not known. The coefficient of sliding

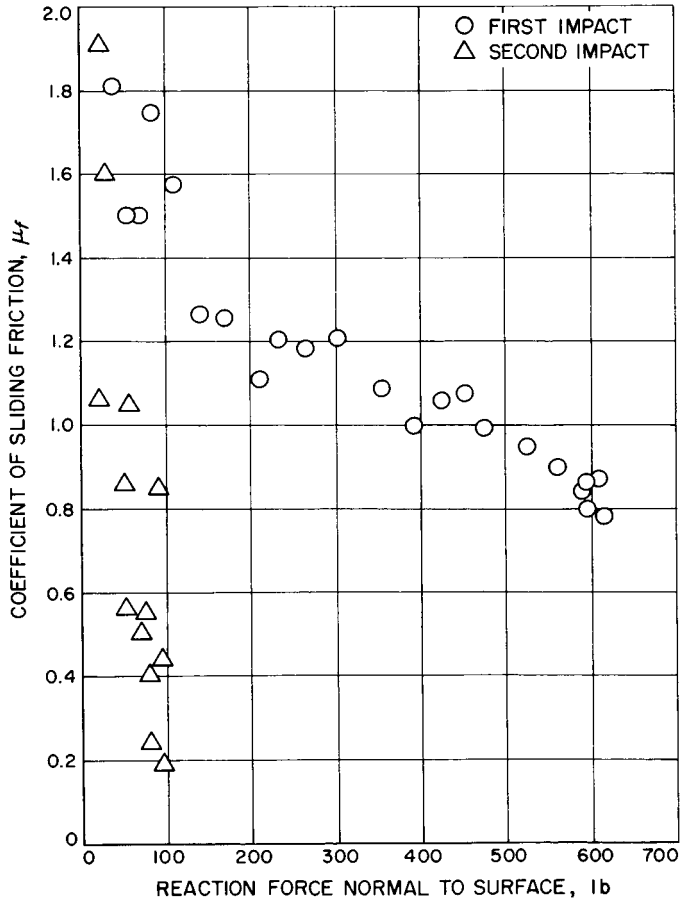

Fig. 9. Coefficient of sliding friction vs reaction force normal to surface; Leg Set No. 2

friction was calculated for all three footpads and the two contacting body blocks. The average body block coefficient of friction, μ_B, was found to be 0.34. Since the body blocks are in contact only a relatively short time, the variation of μ_B with normal force or velocity was not investigated. Figures 8 through 10 show the variation of the coefficient of sliding friction, μ_f, vs the reaction force normal to the surface for each footpad. In drawing conclusions from these curves, it should be remembered that the other variables, such as velocity and contact area, are hidden parameters. There is a tendency, especially on footpads No. 1 and No. 2, for μ_f to decrease with an increasing normal reaction force. It is evident also that the coefficient of sliding friction is smaller for footpad No. 1 than for either footpad No. 2 or No. 3. Footpad No. 1, on the trailing leg, was the first to impact.

The reaction force on footpad No. 1 reached values as high as 910 lb. The aluminum honeycomb material used in the footpad is such that a fully contacting pad starts crushing at approximately 500 lb. Due to the conical shape of the footpad, the crushing force increases to approximately 1000 lb at a crushed height of 2 in. Examination of footpad No. 1 after the test showed that this footpad had crushed substantially less than 2 in. and that it did not contact with its full area, hence exhibiting definite off-axis loading which tends to reduce the crushing strength.

The aluminum honeycomb is not precrushed. Hence, the high normal force is due to dynamic overload. The overload factor on footpad No. 1 reaches a maximum of approximately 1.8.

Figure 11 shows the time histories of the reaction forces on the three different footpads. It is seen that on footpad No. 1 the peak force is of very short duration. The reaction force time history for footpad No. 1 resembles the dynamic behavior of non-precrushed honeycomb very closely. Footpads No. 2 and No. 3 do not exhibit this dynamic overshoot; this is attributed to the difference in footpad orientation, footpad velocity, and the direction of the loading at the time of initial impact. A maximum reaction force of approximately 600 lb is easily explained by considering the effect of geometry on the crushing force of the footpad.

Examining Figs. 8 through 10, it is seen that the scatter in the data seems to increase considerably below a reaction force of 100 lb; this is not unreasonable if the accuracy of force measurement and the sensitivity of the friction coefficient to this accuracy are considered. To

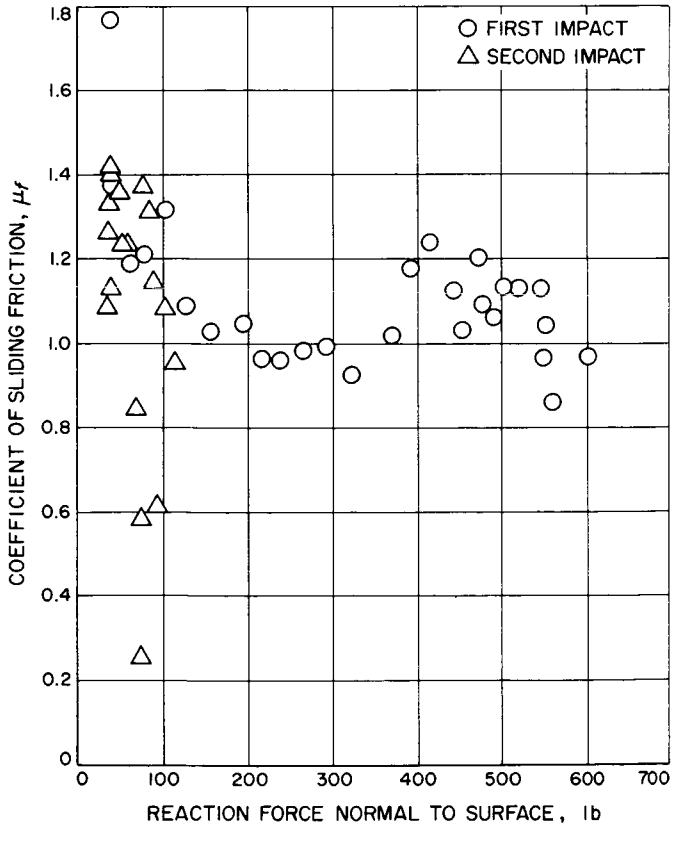

Fig. 10. Coefficient of sliding friction vs reaction force normal to surface; Leg Set No. 3

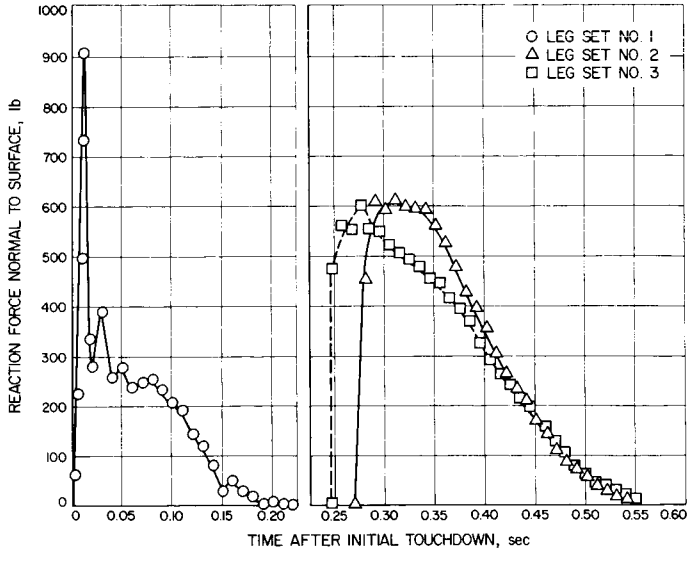

Fig. 11. Time histories of the reaction forces normal to surface

obtain a better appreciation of the data, Fig. 12 shows the variation of the coefficient of sliding friction as a function of the reaction force normal to the surface for all three footpads. Data points corresponding to reaction forces below 100 lb have been omitted.

Since no data are available correlating footpad velocity to time after touchdown, the effect of velocity on μ_f cannot be evaluated directly. Figure 13 shows a plot of the coefficient of sliding friction, μ_f, vs time after initial touchdown. The vehicle velocity, as well as the footpad velocity, decreases with time. To establish a trend for the variation of the coefficient of sliding friction with velocity, μ_f has been plotted as a function of the calculated velocity of the vehicle c.g., Fig. 14. To predict a velocity time history using the computer, a value for μ_f had to be assumed; $\mu_f = 0.90$ was chosen. It should be noted that the velocity of the vehicle c.g. is only an approximation for the local footpad velocity. It should also be remembered that in both Figs. 13 and 14, the reaction force normal to the surface is a hidden variable.

Using Fig. 13 and 14, a general trend can be established: μ_f decreases with increasing velocity. This section shows that the coefficient of sliding friction in this drop test was not a constant, but varied rather widely. Variations with respect to normal force and footpad velocity could be established only qualitatively.

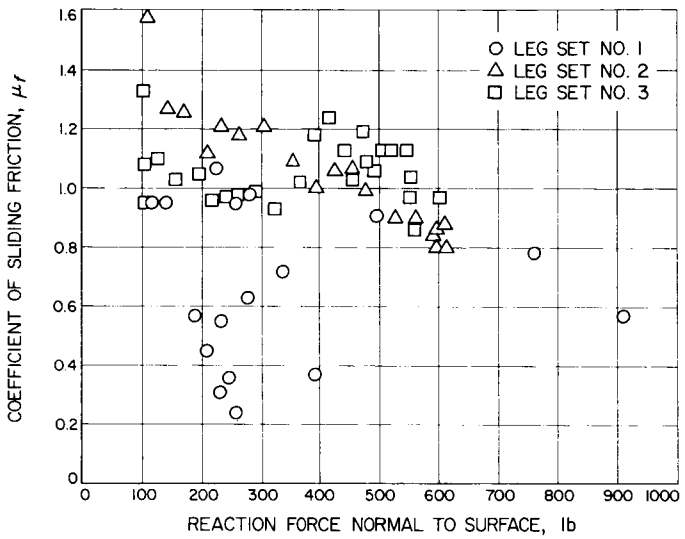

Fig. 12. Coefficient of sliding friction vs reaction force normal to surface

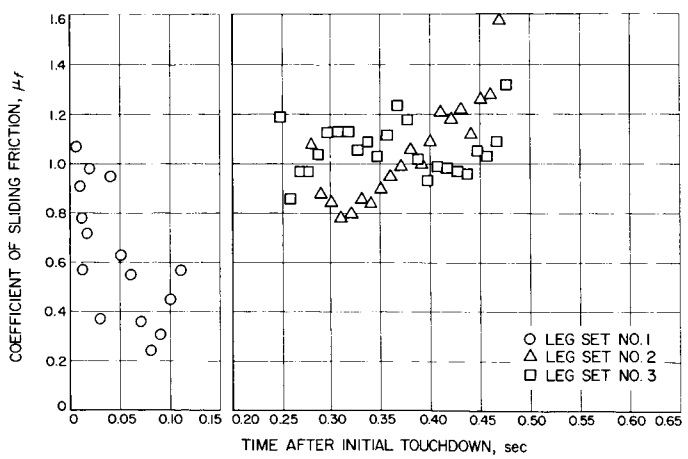

Fig. 13. Coefficient of sliding friction vs time after initial touchdown

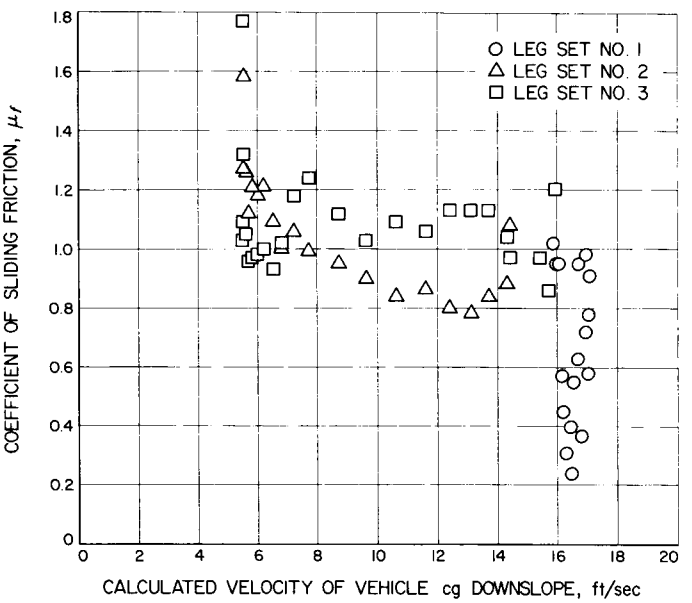

Fig. 14. Coefficient of sliding friction vs calculated vehicle c.g. velocity, downslope

2. Non-steady gravity force. The time history of the "anti-gravity" force, as recorded by the in-line load cell (Fig. 7), is shown in Fig. 15. It is apparent that this is not a constant quantity. There are high-frequency oscillations of approximately ±60 lb which amount to a ±60% variation in the lunar gravity force for this particular test. The mean was found to vary by approximately ±10 lb or ±10% lunar g.

3. Touchdown velocities. There are uncertainties in the prediction of the exact velocities at touchdown. Simple calculations using distances and times from test vehicle

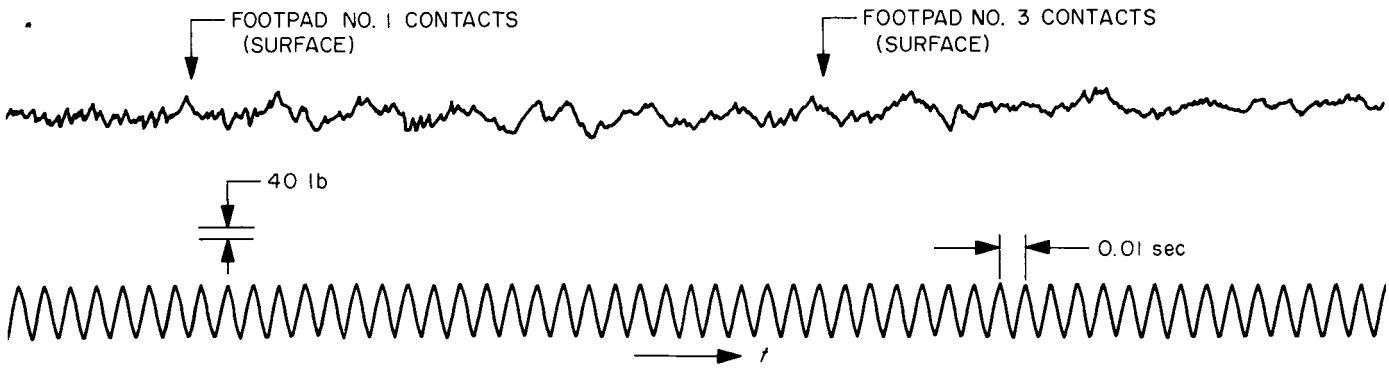

Fig. 15. "Anti-gravity" force time history

release to touchdown indicate the following average velocities in ft/sec for the pre-touchdown flight:

$$v_y = -11.7 \; ; \; v_z = 17.1$$

The above velocities refer to a vehicle fixed coordinate system (see Fig. 4 and 6). Due to the friction in the system, it is safe to assume that the actual touchdown velocities were below these two values.

4. Variations in mass loading due to instrumentation cabling. Coaxial cable was used to transmit the signals from the transducers aboard the vehicle. This cabling, heavy as it was, probably induced more of a force than a mass effect on the system. However, since it is impossible either to measure or correct for it, this effect was neglected in the reduction of test data and in the analytical representation of the drop test.

B. Sensitivity of the Computer Predictions to Test Uncertainties

The sensitivity of a number of dependent variables, namely, the pitch-angle time history, the maximum pitch angle, the maximum pitch rate, and the maximum shock-absorber force for each leg, was studied by numerical evaluation using the computer simulation of the test vehicle as a function of the following parameters: (1) the coefficient of sliding friction for the footpad, (2) the gravitational constant, and (3) the velocities of the c.g. at touchdown. One parameter at a time was varied, while the other parameters were kept fixed at their nominal values. An examination of the test records showed that the vehicle experienced some small change in angular orientation during the pre-touchdown free-flight. This was indicated by the attitude gyros as well as the difference in the impact times between leg No. 2 and leg No. 3. In order to simulate these different impact times in the computer runs, the following initial vehicle attitudes in deg were used:

$$\psi_0 = 10 \; ; \; \phi_0 = 0.9 \; ; \; \Xi_0 = -0.9$$

1. Effect of variations of the coefficient of sliding friction for the footpads. Due to the large variation of μ_f during the test, as exhibited by Fig. 12 through 14, the effect of μ_f in the region from $\mu_f = 0.7$ to $\mu_f = 1.2$ was investigated.

Since for a planar drop, as the one being investigated, the pitch angle is a direct indication of vehicle stability, the pitch-angle time history was studied in detail. The result of this computer investigation is shown in Fig. 16. It is seen that the vehicle stability is a very sensitive function of μ_f. The vehicle is predicted to be unstable for $\mu_f = 1.2$, $\mu_f = 1.0$, $\mu_f = 0.95$, and stable for $\mu_f = 0.9$ and smaller values of μ_f. The result for $\mu_f = 0.925$ warrants further discussion. By examining the pitch-angle time histories of Fig. 16, one conclusion is that once the vehicle pitch angle exceeds approximately 23 deg it will topple. If it does not reach 23 deg, it will be stable. This is not physically reasonable, as it would be expected that the decision of vehicle stability or instability would fall closer to the pitch angle of statically neutral stability, or approximately 52 deg. The pitch-angle time history for $\mu_f = 0.925$, shown in Fig. 17, proves this intuitive reasoning to be correct. Here, the maximum pitch angle reached is 45 deg, and the vehicle rocks back to a stable condition.

Based on the good agreement between the test results and $\mu_f = 0.9$, as shown in Fig. 15, this value of μ_f was selected as the best choice for the coefficient of sliding friction. In studying the effect of variations in the gravitational constant and the initial velocities, to be discussed later, μ_f was held constant at 0.9.

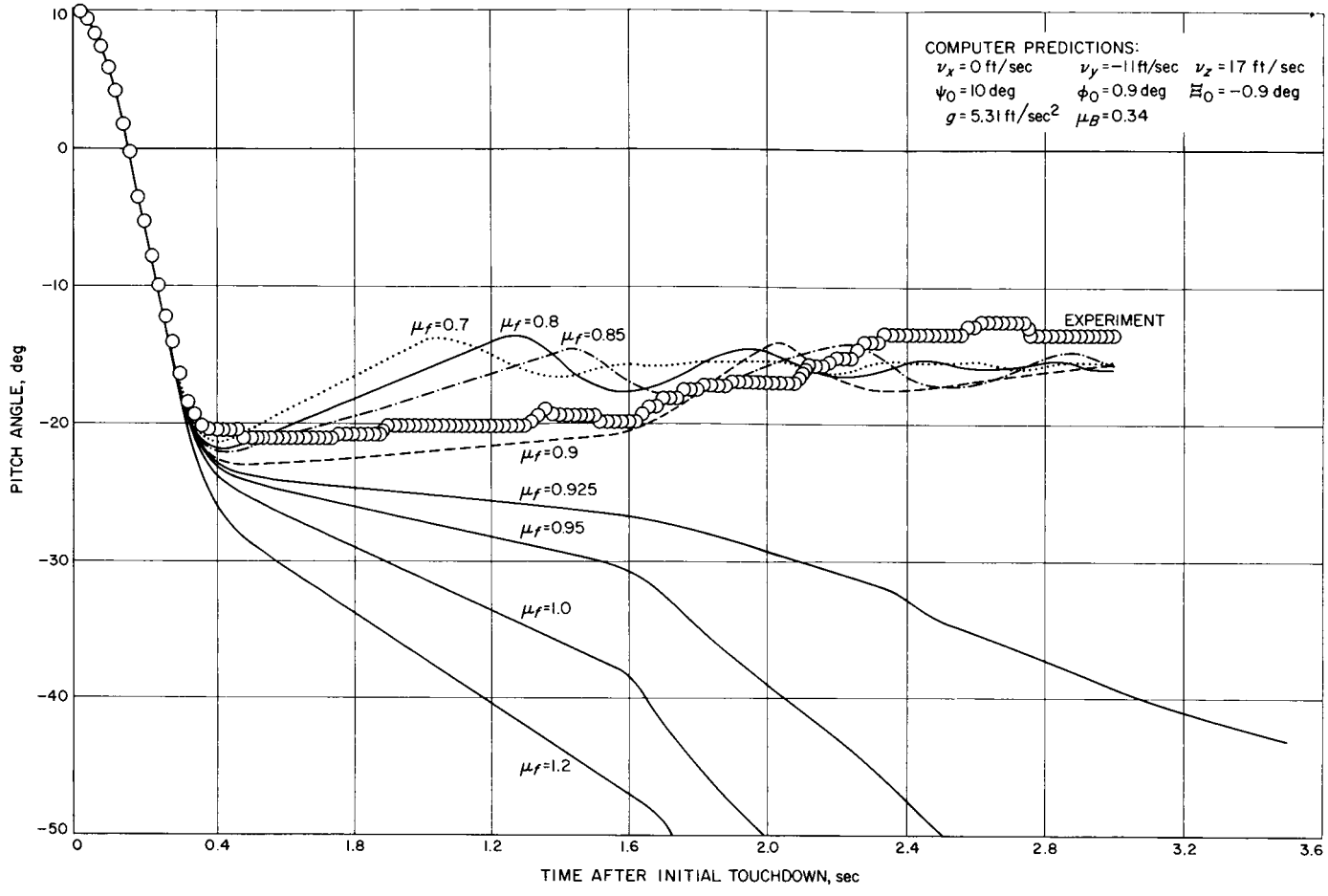

Fig. 16. Pitch-angle time histories for various coefficients of sliding friction

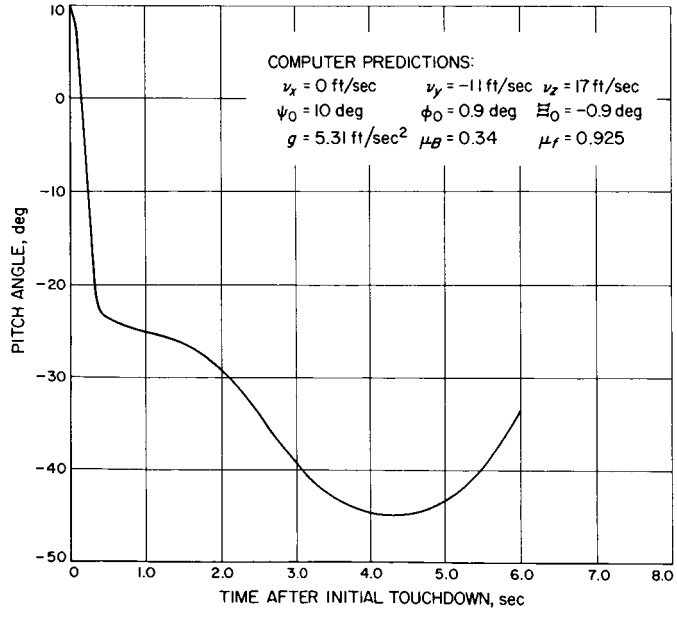

Fig. 17. Pitch-angle time history for μ_f = 0.925

Another indication of the effective coefficient of friction is the total slide distance during the test. Table 2 shows the effect of μ_f on the horizontal c.g. location, Y. Based on the parametric values of this table alone, it would be concluded that for computational purposes a coefficient of sliding friction larger than 0.925 should be used. This contradicts previous findings (Fig. 16) since an unstable vehicle would result.

The rationale for this contradiction is as follows. There are friction forces acting in the test setup at places other than the footpads. Certainly the friction forces acting in the rolling pulley (Fig. 7) tend to retard the vehicle. Forces induced through the instrumentation cabling, discussed under Section IV-A-4 above, would also retard the vehicle. Since these forces are not accounted for in the computer simulation, a discrepancy between Fig. 16 and Table 2 is likely to result. Table 3 shows the effect of the coefficient of friction on the maximum pitch rate and the maximum shock-absorber forces. It is seen that μ_f has very little effect on the maximum pitch rate, ω_x.

Table 2. Effect of variations in the effective coefficient of friction on the horizontal c.g. location

μ_f	Y (at t = 3 sec) (ft)
0.7	23.6
0.8	19.7
0.85	17.3
0.9	15.3
0.925	14.0
Test	11.1 (Final position of vehicle)

Computed results of the S-15 test vehicle: $v_x = 0$ ft/sec; $v_y = -11$ ft/sec; $v_z = 17$ ft/sec; $\psi_0 = 10$ deg; $\phi_0 = 0.9$ deg; $\Xi_0 = -0.9$ deg; $\mu_B = 0.34$; $\theta_s = 15$ deg.

Table 3. Effect of variations in the effective coefficient of friction on the maximum pitch rate and shock-absorber forces

μ_f	0.7	0.8	0.85	0.9	0.925	0.95	1.0	1.2
$\omega_{x\ max}$ (deg/sec)	−121	−122	−122	−123	−123	−123	−123	−124
$F_{1\ max}$ (lb)	1340	1370	1370	1380	1380	1390	1410	1430
$F_{2\ max}$ (lb)	2790	2920	3200	3280	3080	3120	3180	3690

Computed results of the S-15 test vehicle: $v_x = 0$ ft/sec; $v_y = -11$ ft/sec; $v_z = 17$ ft/sec; $\psi_0 = 10$ deg; $\phi_0 = 0.9$ deg; $\Xi_0 = -0.9$ deg; $\mu_B = 0.34$; $\theta_s = 15$ deg.

The maximum force in the shock absorber of leg No. 1, F_1, consistently increases with increasing μ_f. The shock-absorber force in leg No. 2, F_2, increases with increasing μ_f for both the stable and unstable cases with a pronounced discontinuity at $\mu = 0.925$, the marginal case.

In evaluating the effects of variations of μ_f on the parameters described above, it should be kept in mind that the computer simulation treats the friction coefficient as essentially constant. Details of how the friction coefficient is handled in the program are described in Appendix B. While the above discussion essentially brackets the variation in μ_f seen in the test, it does not account for the transient behavior of the friction coefficient nor does it account for the difference in μ_f for different footpads.

2. Effect of variations in the gravitational constant. Table 4 shows the effect of a variation of ±20% and ±60% on the value of the gravitational constant on the maximum pitch angle, maximum pitch rate, and maximum shock-absorber forces. It is seen that a large variation in g has a rather small effect on both the maximum pitch angle and pitch rate. The maximum force in shock-absorber No. 1 is not affected appreciably. The variation of the maximum force in shock-absorber No. 2 merits some discussion. Table 4 shows that F_2 is increasing with increasing g, but this increase has a discontinuity between $g = 5.31$ ft/sec² and $g = 6.37$ ft/sec.² Examination of the detailed time-history printout showed that for $g = 2.12$ ft/sec², $g = 4.25$ ft/sec² and $g = 5.31$ ft/sec.² The shock-absorber forces F_2 and F_3 were allowed to

Table 4. Effect of variations in the gravitational constant on the maximum pitch angle, pitch rate, and shock-absorber forces

g (ft/sec²)	2.12	4.25	5.31	6.37	8.42
ψ_{max} (deg)	−28	−26	−23	−23	−22
$\omega_{x\ max}$ (deg/sec)	−119	−121	−123	−124	−127
$F_{1\ max}$ (lb)	1380	1380	1380	1380	1390
$F_{2\ max}$ (lb)	2870	2940	3280	3170	3390

Computed results of the S-15 test vehicle: $v_x = 0$ ft/sec; $v_y = -11$ ft/sec; $v_z = 17$ ft/sec; $\psi_0 = 10$ deg; $\phi_0 = 0.9$ deg; $\Xi_0 = -0.9$ deg; $\mu_B = 0.34$; $\mu_f = 0.9$ deg; $\theta_s = 15$ deg.

build up to their maximum force before the body blocks contacted; that is, the body blocks contacted at a time when the shock-absorber forces were decreasing. For $g = 6.37$ ft/sec² and $g = 8.42$ ft/sec², the body blocks contacted at a time when F_2 and F_3 were still increasing, thus redistributing the forces acting on the spacecraft and limiting the maximum shock-absorber forces. If the body blocks were removed $F_{2\,max}$ would increase with increasing g.

One other effect of the variation of the gravitational constant which is very important but does not show up in Table 4 is the motion of the vehicle after legs No. 2 and No. 3 rebound. While the times for the first impact

of leg No. 2 and No. 3 are relatively insensitive to a variation in g of $\pm 20\%$, the re-impact times for all three legs and the re-impact frequencies are quite different, resulting in a completely different vehicle displacement time history. It should also be noted that the computer simulation does not provide for a transient behavior of the gravity force as observed in the test (Fig. 15).

3. Effect of variations of the velocities at touchdown.

a. Variations in the horizontal velocity at touchdown. Table 5 shows that a variation of ± 1 ft/sec in horizontal velocity has an insignificant effect on the maximum pitch rate. The maximum shock-absorber force in leg No. 1

Table 5. Effect of variations in the horizontal velocity at touchdown on the maximum pitch angle, pitch rate, and shock-absorber forces

V_H (ft/sec)	12.8	13.8	14.8
ψ_{max} (deg)	−23	−23	−23
$\omega_{x\ max}$ (deg/sec)	−125	−123	−121
$F_{1\ max}$ (lb)	1410	1380	1350
$F_{2\ max}$ (lb)	3130	3280	2960

Computed results of the S-15 test vehicle: $v_x = 0$ ft/sec; $v_z = 17$ ft/sec; $\psi_0 = 10$ deg; $\phi_0 = 0.9$ deg; $\Xi_0 = -0.9$ deg; $\mu_B = 0.34$; $\mu_f = 0.9$; $g = 5.31$ ft/sec^2; $\theta_s = 15$ deg.

decreases with increasing horizontal velocity. This is attributable to the geometry; that is, the horizontal velocity component tends to relieve the shock-absorber force in leg No. 1. An increase in horizonal velocity does tend to increase the shock-absorber forces in leg No. 2 and No. 3. For the case of $V_v = 14.8$ ft/sec, the body blocks impact while F_2 is still increasing.

b. Variations in the vertical velocity at touchdown. The effect of varying the vertical velocity by ± 1 ft/sec on the maximum pitch angle, pitch rate, and shock-absorber forces is shown in Table 6. Here again, it is seen that the pitch angle and pitch rate are not significantly affected. All maximum shock-absorber forces increase with an increase in vertical velocity; this is to be expected. For the $V_v = 15.8$ ft/sec case, the body blocks impacted at a time when the shock absorber forces F_2

Table 6. Effect of variables in the vertical velocity at touchdown on the maximum pitch angle, pitch rate, and shock-absorber forces

V_V (ft/sec)	13.8	14.8	15.8
ψ_{max} (deg)	−24	−23	−22
$\omega_{x\ max}$ (deg/sec)	−115	−123	−131
$F_{1\ max}$ (lb)	1250	1380	1520
$F_{2\ max}$ (lb)	2700	3280	3630

Computed results of the S-15 test vehicle: $v_x = 0$ ft/sec; $v_y = -11$ ft/sec; $\psi_0 = 10$ deg; $\phi_0 = 0.9$ deg; $\Xi_0 = -0.9$ deg; $\mu_B = 0.34$; $\mu_f = 0.9$; $g = 5.31$ ft/sec^2; $\theta_s = 15$ deg.

and F_3 were increasing. It is seen from Table 6 that F_2 is rather sensitive to variations in V_v.

4. Summary. In this section an attempt has been made to show the variation in certain computed output variables to be expected due to uncertainties in the input. The input was varied within the limits experienced during the test.

It should again be emphasized that parameters, such as the gravitational constant and the coefficient of sliding friction, are treated as constants in the computer simulation while they were found to be time dependent in the actual test. Even though the encountered uncertainties were bracketed, it is conceivable that due to transient phenomenon the observed test results could fall outside the predicted ranges. Also, no attempt was made to study the effect of varying more than one input parameter at a time. It is tacitly assumed that in studying the effects of the test uncertainties on the computer predictions, the variations in these predictions can be combined linearly.

V. Comparison of Time Histories Obtained from a Drop Test to Those Predicted by the Computer Program

The results of the previous section are used to establish the input parameters to the computer program such that experimental and theoretical time-history plots can be correlated.

Based on the results shown in Fig. 16, it was decided to use a coefficient of sliding friction for the footpads, μ_f, of 0.9. The friction coefficient for the body blocks, μ_B, was established as 0.34. Since the variation of the gravitational constant, as shown in Fig. 15, was rather large, it was decided to use the nominal value. The touchdown velocities calculated from average times and distances were close to the nominal values; hence, the nominal values were used. The nominal vehicle inertial properties were used as an input to the computer program.

Detailed test data on the shock-absorber characteristics employed in this test were not available. Nominal characteristics, as specified in the design criteria, were used for the shock-absorber damping coefficients, spring constants, and their associated profiles; these are summarized in Appendix A.

The parameters used as input to the computer for the case to be compared to the drop test results are summarized below:

$$v_x = 0\,; \qquad v_y = -11 \text{ ft/sec}\,; \qquad v_z = 17 \text{ ft/sec};$$

$$\psi_0 = 10 \text{ deg}\,; \qquad \phi_0 = 0.9 \text{ deg}\,; \qquad \Xi_0 = -0.9 \text{ deg};$$

$$\mu_f = 0.9; \qquad \mu_B = 0.34\,;$$

$$\theta_S = 15 \text{ deg}; \qquad g = 5.3 \text{ ft/sec}^2$$

As discussed earlier, the vehicle motion after leg No. 2 and leg No. 3 rebound is very sensitive to the magnitude of the gravitational constant used. Therefore, the time histories will be compared to 0.6 sec. The effect of the non-constant gravitational force, due to the mechanization of the "anti-gravity" device, becomes more pronounced after the spacecraft vertical velocity reverses its sign. This occurred, according to computer predictions, at 0.39 sec after touchdown.

In all the time-history plots of this section, the test results are shown as discreet points represented by dots and circles. These points were obtained by reading the values of the variables from the continuous test oscillograph records.

A. Pitch-Angle Time History

The comparison between the actual and the predicted time history is shown in Fig. 18. It was seen earlier that the pitch-angle time history is very sensitive to the coefficient of friction used in the computer simulation.

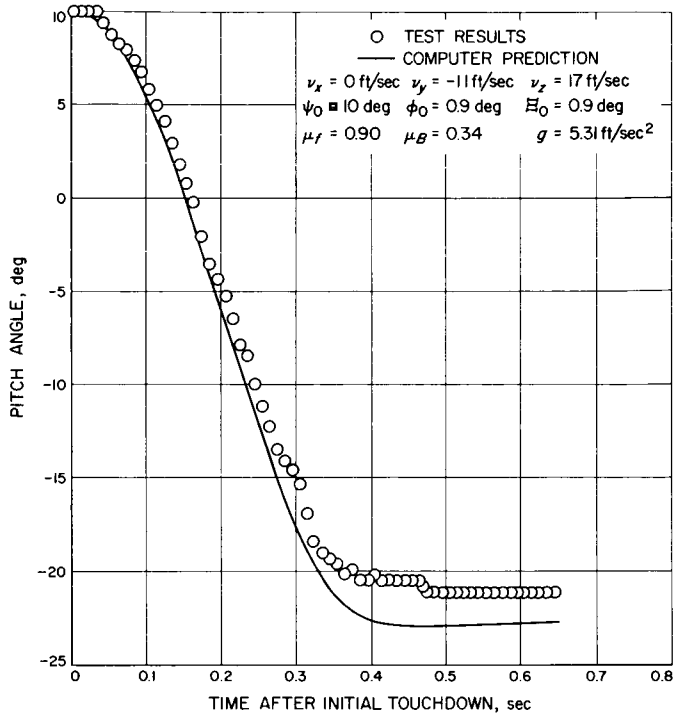

Fig. 18. Pitch-angle time history

In the time duration shown, the computed pitch angle is differing from the measured angle by a maximum of 7.5%. This is a rather good correlation.

B. Pitch-Rate Time History

The two pitch-rate time histories are shown in Fig. 19. It is seen that the maximum test pitch rate is about 40 deg/sec lower than the predicted pitch rate. An integration of the test pitch rate indicates that the maximum value of the pitch angle obtained in this fashion is about 10 deg more positive than the one indicated by either the position gyro or the computed predictions. This discrepancy is attributable to the frequency response of the transducer.

C. Shock-Absorber Force Time Histories

The shock-absorber force time histories for both test and computer prediction for all three legs are shown in Fig. 20 through 22.

Figure 20 shows that the peak for F_1 is sharper in the computer prediction. The predicted and measured forces in shock-absorber No. 1 correlate very well.

Figures 21 and 22 do not show such good agreement. It should be noted that the initial slope on both of these

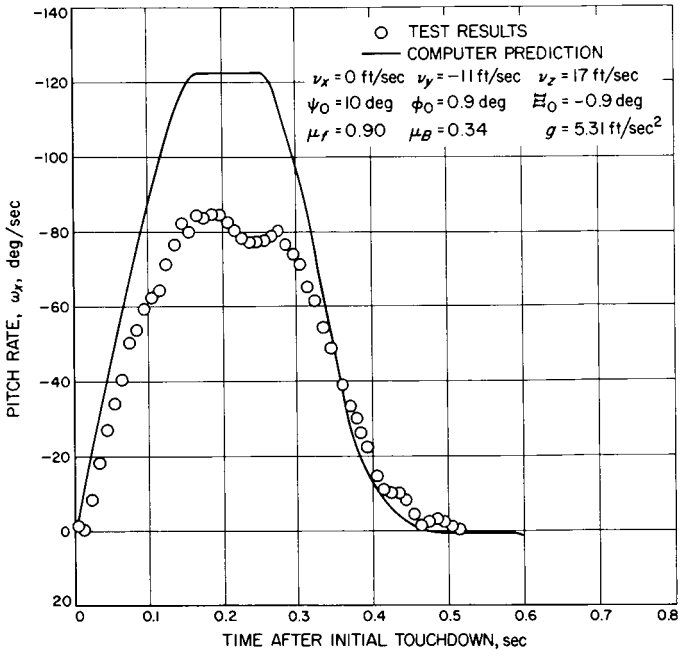

Fig. 19. Pitch-rate time history

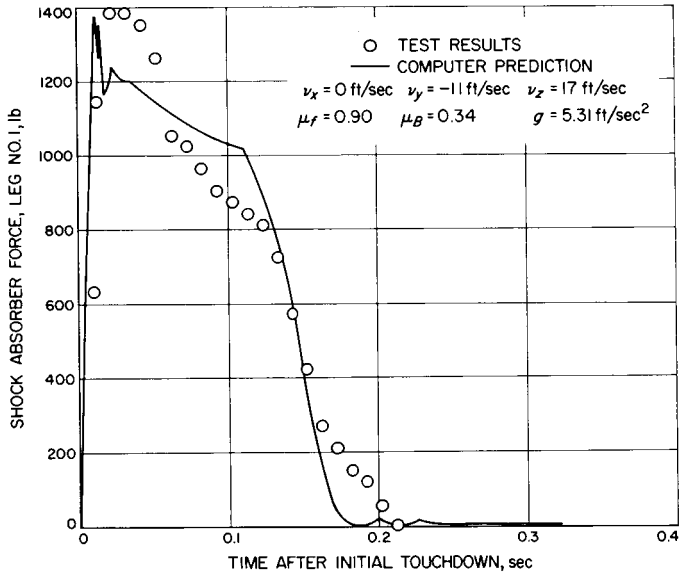

Fig. 20. Shock-absorber time history, Leg No. 1

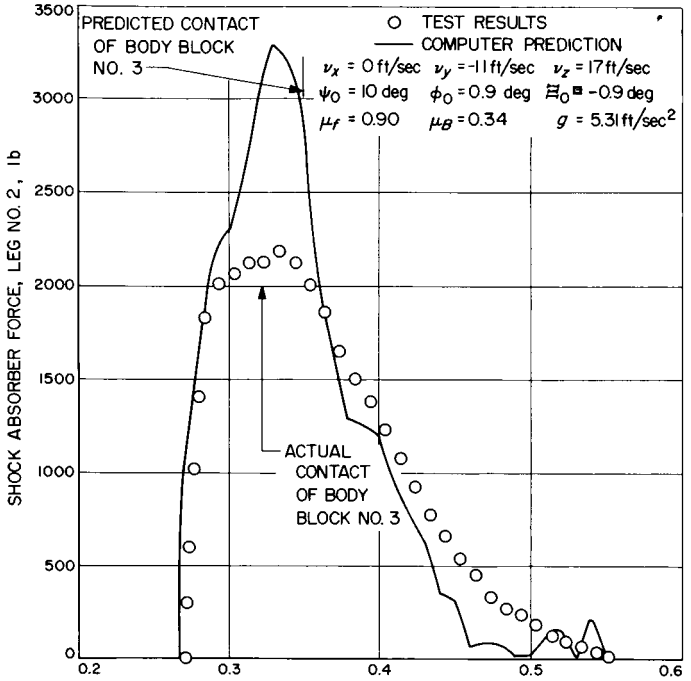

Fig. 21. Shock-absorber time history, Leg No. 2

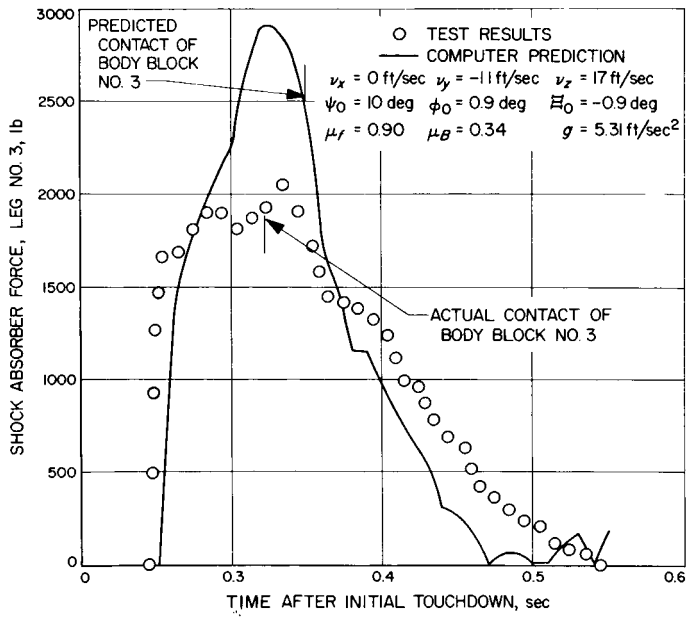

Fig. 22. Shock-absorber time history, Leg No. 3

curves agrees well with the test results. This tends to indicate that the elasticity of the landing legs has been modeled properly in the computer program.

The difference in maximum force for F_2 and F_3 can be explained in part by examining the impact times of the body blocks. As was noted earlier, these impact times are rather sensitive to the value of the gravitational constant, and the vertical and horizontal velocity at touchdown. In the computer, both F_2 and F_3 are allowed to build up to their respective maxima before the body blocks impacted. In the drop test the maximum force in each shock absorber is reached at approximately the

same time as the body blocks impact. Thus, the body-block impact limits the shock-absorber maximum force. During the test, body-block No. 3 impacted 23 msec before the predicted time. The fact that the agreement for the maximum force in shock-absorber No. 1 is so much better does confirm that the body-block impact times are affecting the maximum shock-absorber forces.

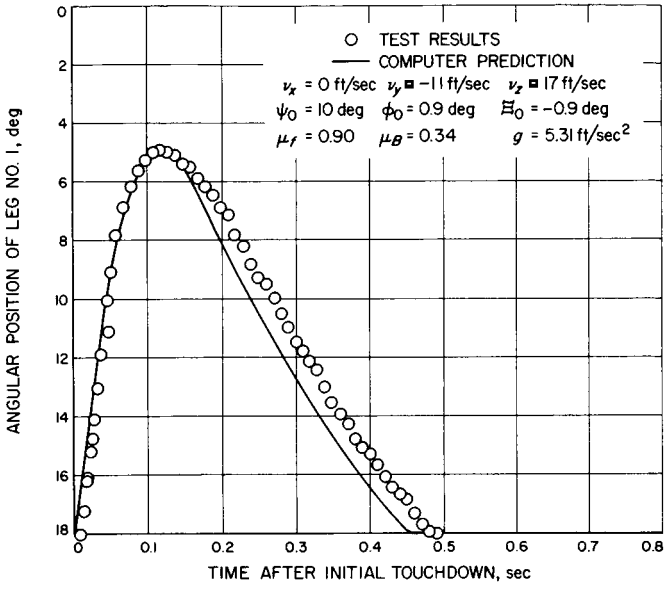

Fig. 23. Angular-position time history, Leg No. 1

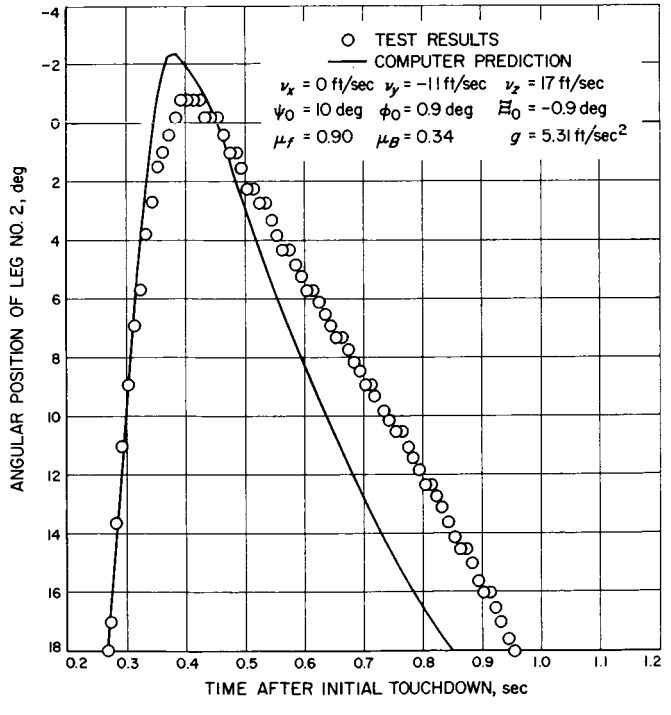

Fig. 24. Angular-position time history, Leg No. 2

D. Leg-Deflection Time Histories

The leg-deflection time histories are shown in Fig. 23 through 25. These results show good agreement between test and computed data on the upstroke with variations of approximately one degree. On the downstroke, discrepancies as high as three degrees are noted. Nominal shock characteristics were used for all shock absorbers since no test data were available for the hardware used. On the flight hardware of *Surveyor I*, it was found that the shock-absorber characteristics describing the rebound differed substantially from the nominal values. All three of the flight shock absorbers had a rebound damping coefficient as well as a rebound profile slope which was higher than the nominal value. If it is assumed that the shock absorbers used in this test exhibit similar characteristics, the discrepancy in leg position during the downstroke is explained.

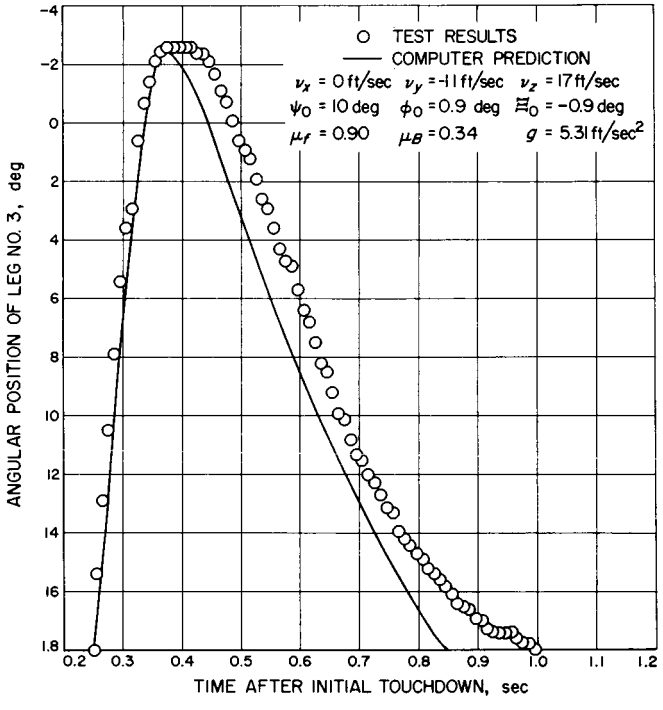

Fig. 25. Angular-position time history, Leg No. 3

The best correlation is shown for leg No. 1. This is in line with F_1 showing the best correlation among the shock-absorber time histories.

E. Lower-Strut Moment Time Histories

As described in Section II, the lower strut of each leg, pivoted from the spaceframe, is capable of carrying a

moment in its own plane. Since the drop test being discussed was basically symmetric, the measured as well as the predicted moment in lower strut No. 1 was small and will not be compared. The lower-strut moment histories for legs No. 2 and No. 3 are shown in Fig. 26 and 27, respectively.

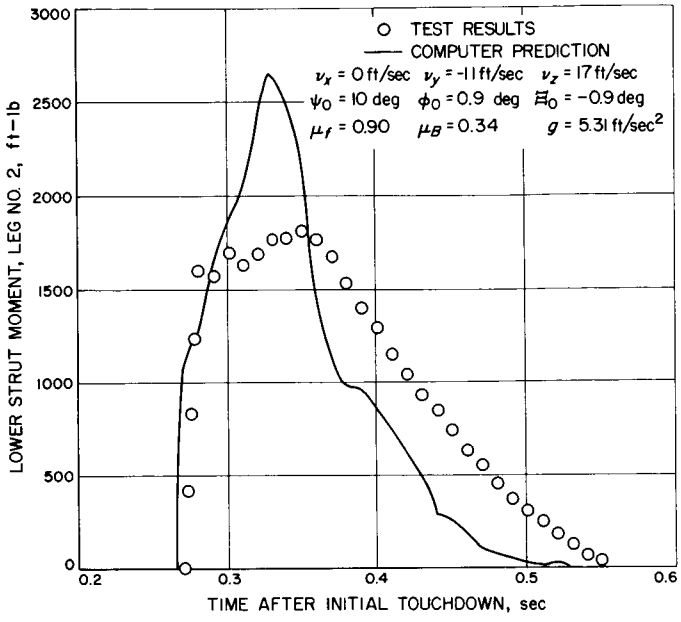

Fig. 26. Lower strut moment, Leg No. 2

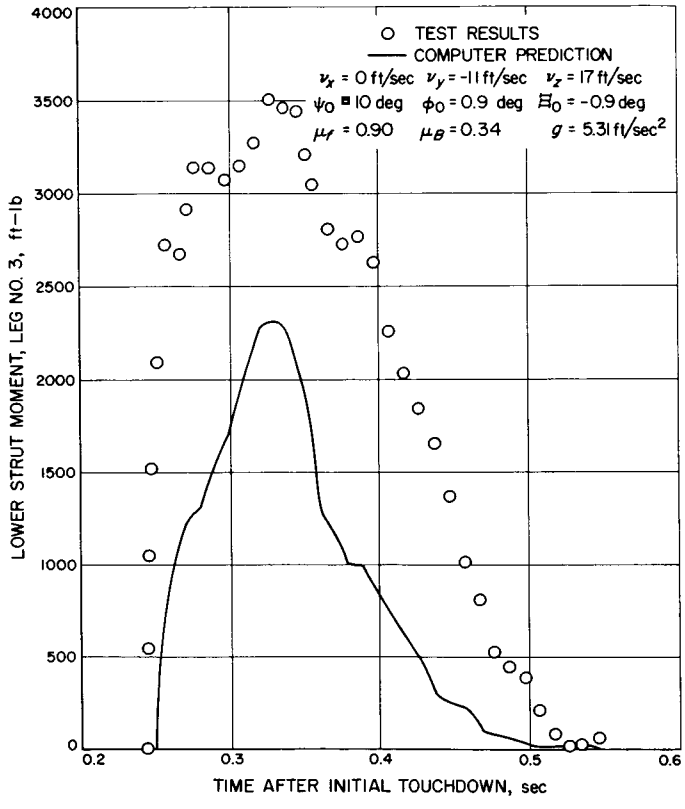

Fig. 27. Lower strut moment, Leg No. 3

A comparison of the moment of strut No. 2 to that of strut No. 3 shows the nonsymmetry of the drop test. The average of the two maximum moments is close to what the predicted values show. The discrepancy in the maximum lower-strut moments of the two struts is consistent with the final vehicle orientation. The final vehicle orientation as determined from the attitude gyro output in deg was as follows:

$$\text{Pitch} = -13.5$$

$$\text{Yaw} = -8.5$$

$$\text{Roll} = -12.0$$

For a completely symmetrical drop, both roll and yaw should be zero and the pitch should be -15 deg.

The computer accounted for the initial yaw and roll using $\phi_0 = 0.9$ deg and $\Xi_0 = -0.9$ deg. The yaw and roll time histories from the computer predictions account

Table 7. Times of major events

Event	Time after touchdown, sec	
	Predicted	Actual
Leg 1 rebounds	0.175	0.213
Leg 3 contacts	0.250	0.240
Leg 2 contacts	0.266	0.267
Body block 3 contacts	0.350	0.323
Body block 2 contacts	0.354	0.340
Body block 3 rebounds	0.375	0.410
Body block 2 rebounds	0.385	0.420
Leg 2 rebounds	0.525	0.553
Leg 3 rebounds	0.525	0.543
First "free-flight" starts	0.175	0.213
First "free-flight" terminates	0.250	0.240

Computed results of the S-15 test vehicle: $v_x = 0$ ft/sec; $v_y = -11$ ft/sec; $v_z = 17$ ft/sec; $\psi_0 = 10$ deg; $\phi_0 = 0.9$ deg; $\Xi_0 = -0.9$ deg; $\mu_B = 0.34$; $\mu_f = 0.9$ deg; $\theta_s = 15$ deg.

for an asymmetry of only a few degrees. The major contribution to this asymmetry comes from the forces induced through the instrumentation cabling. These forces are not accounted for in the computer simulation.

F. Times of Major Events

The times of the major events are summarized in Table 7. A few observations can be made by examining this table.

The initial contact times of the footpads are predicted rather well. All the appendages of the test vehicle stay in contact with the ground longer than predicted. This is due to the non-realistic shock-absorber profiles used in the analysis and the non-constant "anti-gravity" force of the test rig. The actual "free-flight" time is shorter than the predicted one.

VI. Conclusions

The objectives of the *Surveyor* S-15 drop-test program were two-fold:

1. To establish correlation between test and analysis.
2. To insure that the *Surveyor* stability margins fall within the expected spacecraft performance during a lunar landing.

Both of these objectives require a testing program wherein the parameters affecting the detailed vehicle behavior are well controlled. If, as was the case for the *Surveyor* spacecraft, it is determined during the drop-test program that the expected performance falls well within the stability boundary, the second objective can be met with relaxed requirements on the control of critical variables. Unfortunately this is not true of the first objective.

Any conclusions drawn from the comparison of predicted behavior to test behavior of the vehicle as shown in Section V must consider the effect of the test uncertainties as discussed in Section IV.

While it seems inconsistent to select a coefficient of friction to be used in the computer program from a pitch-angle time history investigation as the one shown in Fig. 16, it is a practical approach in view of the variations of μ_f as seen in Fig. 12 through 14 and the computer simulation for the coefficient of friction, Appendix B. Since the time variance of the friction force cannot be accounted for in the program, its effect is not known. Table 3 shows the sensitivity of $F_{2\,max}$ to μ_f. The difference in $F_{2\,max}$ between $\mu_f = 0.7$ and $\mu_f = 0.9$ is 490 lb. This alone could account for a large part of the discrepancy between prediction and test, shown in Fig. 21.

The computer formulation is limited by the treatment of a constant gravity force, which is quite realistic for a lunar landing but not realistic for the gravity simulation used in the test. Due to the effect of g on the impact times of the body blocks and in turn the sensitivity of $F_{2\,max}$ to these impact times, the time variance of g can substantially influence $F_{2\,max}$. It is also noted that for both an increase or decrease of g from the nominal value, the computed prediction for $F_{2\,max}$ decreases, approaching the measured value.

A low vertical velocity at touchdown by 1 ft/sec, shown in Table 6, can account for as much as 580 lb discrepancy in $F_{2\,max}$. It should be noted, however, that the assumption of a low vertical touchdown velocity would increase the difference between the measured and predicted body-block impact times. The computer simulation considers a non-flexible main body. Thus, the program does not account for any energy dissipated in the structure. Even though the test vehicle structure (Fig. 5) is rather rigid, much more so than the flight spacecraft (Fig. 1), it does dissipate some energy in the elastic structure upon impact. Such energy dissipation does reduce the maximum shock-absorber forces.

In view of all these uncertainties, the time-history correlation shown in Section V is good. Unfortunately, the value and necessity of some refinements in the mathematical model, such as the treatment of the leg set and the footpad, could not be confirmed by these tests. In view of the difficulties of controlling some of the parameters in this test, an alternate test method should be considered.

In order to avoid the difficulty of simulating lunar gravity, dynamic modeling could be used. This was investigated extensively by the Hughes Aircraft Company. The results are described in Ref. 3. Difficulties were encountered in modeling the shock absorber. A properly-scaled shock strut resulted in a mass distribution which was unrealistic. Dynamic modeling was not feasible.

For the velocities of interest in the investigation of stability margins, the full-size vehicle cannot be dropped

under Earth gravity due to the inability of the legs to support the spacecraft after landing. Also, the effect of the Earth gravity as compared to Moon gravity results in an undesirable increase in landing stability.

For a full-size vehicle, various methods for simulating lunar gravity were considered by the Hughes Aircraft Company. These are described in Ref. 3. The method most favorable from a dynamic point of view is the dropping platform. The full-size unrestrained test vehicle is allowed to drop under Earth gravity onto a platform accelerating at 5/6 Earth g, such that the test vehicle's acceleration relative to the platform is that of lunar gravity. Due to the size of the required test facility, this method was considered economically unfeasible.

In order to eliminate the variations in the coefficient of friction, the footpads could be replaced by metal spikes, resulting in essentially an infinite coefficient of friction.

Despite the limitations described above, the two objectives could be met by:

1. Dropping the full-size vehicle, unrestrained, under Earth gravity at velocity combinations not detrimental to the landing gear; the footpads should be replaced by metal spikes; data from these tests would serve to establish correlation between test and analysis; however, the mathematical representation of the footpad could not be checked.
2. Dropping the vehicle using the "anti-gravity" device, described in Section III, at velocity combinations required to establish stability profiles; the footpads should be replaced by metal spikes; all instrumentation requiring external cabling should be removed; Data from these tests in conjunction with computer stability predictions would insure that the *Surveyor* stability margins fall within the expected spacecraft performance during lunar landing.

References

1. Fisher, W. T., *S-15 Lunar Landing Stability Drop-Test Program,* Report SSD 68190R, Space Systems Division, Hughes Aircraft Company, Culver City, Calif., September 1966.
2. Alderson, R. G., and Wells, D. A., *Final Report on Surveyor Lunar Touchdown Stability Study,* Report MM-66-19, Bendix Products Aerospace Division, South Bend, Indiana, July 8, 1966.
3. Deitrick, R. E. and Jones, R. H., *Touchdown Dynamics Study (Preliminary Report), Surveyor Spacecraft System,* Report SSD 3030R, Space Systems Division, Hughes Aircraft Company, Culver City, California, January 1963.

Appendix A
Landing-Gear Characteristics

This Appendix describes the landing-gear characteristics as they are modeled in the computer.

I. Shock-Absorber Characteristics

After the initial compressive strain due to the preload is overcome, the shock-absorber force is given by

$$F_s = K_D S_k\left(\delta - \frac{F_p}{K_s}\right) + F_p - \nu\frac{\dot{\ell}_D}{|\dot{\ell}_D|}\left| K_D\, S_k\left(\delta - \frac{F_p}{K_s}\right) + F_p\right| - \dot{\ell}_D \,|\, \dot{\ell}_D \,|\, R_D\, S_D$$

where

F_s = total shock-absorber force, lb

K_D = spring constant of hydraulic spring, lb/ft

S_k = profile to give nonlinearity of spring constant as a function of shock-absorber stroke, dimensionless

δ = deflection of shock absorber, ft

F_p = hydraulic spring compressive preload, lb

K_s = axial stiffness of strokable strut, lb/ft

ν = mechanical-friction coefficient of shock-absorber moving parts, dimensionless

$\dot{\ell}_D$ = rate of change of shock-absorber length, ft/sec

R_D = damping constant, lb-sec^2/ft^2

$R_D = R_c$ for compression

$R_D = R_R$ for rebound

S_D = profile to give nonlinearity of damping constant, dimensionless

$S_D = S_c$ for compression

$S_D = S_R$ for rebound

The following numerical values were used in the computer simulation to describe the shock-absorber characteristics:

K_D = 3600 lb/ft

F_p = 185 lb

K_s = 100,000 lb/ft

R_c = 54 lb-sec^2/ft^2

R_R = 864 lb-sec^2/ft^2

ν = 0.05

The profiles S_k, S_c and S_R are shown in Fig. A-1. The profiles S_c and S_k are supplied in tabular form as follows:

Shock-absorber deflection (in.)	S_k	S_c
0	1.0	1.0
0.25	1.0	1.08
0.50	1.0	1.16
0.75	1.0	1.24
1.00	1.0	1.36
1.25	1.0	1.48
1.50	1.0	1.60
1.75	1.005	1.74
2.00	1.012	1.89
2.25	1.020	2.13
2.50	1.028	2.77
2.75	1.036	3.81
3.00	1.044	4.96
3.25	1.052	6.09
3.50	1.062	7.24
3.75	1.078	8.37
4.00	1.096	9.52
4.25	1.114	10.67
4.50	1.151	11.80
6.50	1.447	20.84

Linear interpolation is used between the listed values.

The profile S_R is specified as a straight line having a value of 1.0 at zero deflection and a slope of 1.776 ft.$^{-1}$

The constants and profiles given above apply to each of the three shock absorbers.

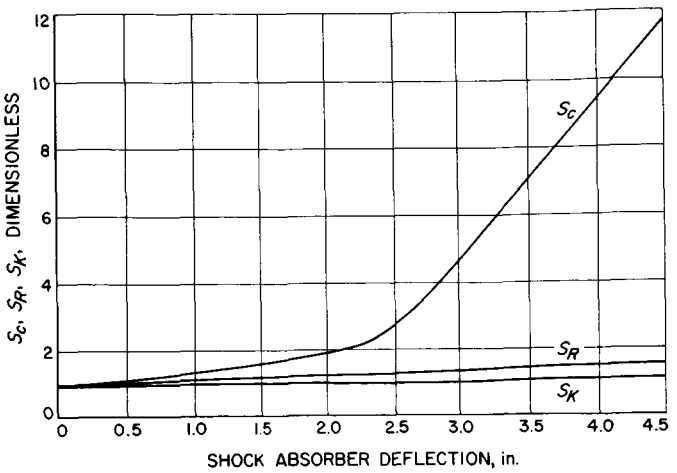

Fig. A-1. Shock-absorber spring and damping profiles

II. Footpad Characteristics

The crush force acting on any segment of a footpad is given by

$$F_f = A_c C_f P_c \left(\frac{0.75 + 0.25 \cos 2\xi_f}{\cos \xi_f} \right)$$

where

F_f = crush force acting normal to the ground surface, lb

A_c = contact area, ft²

C_f = nominal crushing strength per unit area, lb/ft²

P_c = profile to give variation in crushing strength per unit area with displacement, dimensionless

ξ_f = angle of applied load from crushable structure axis, deg

The following numerical values were used in the computer simulation to describe the footpad characteristics:

$$C_f = 1578.8 \text{ lb/ft}^2$$

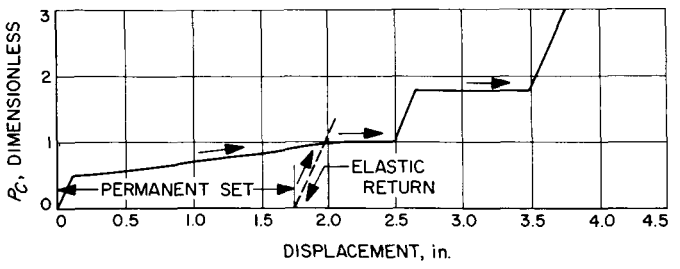

Fig. A-2. Footpad crush-pressure profile

The profile P_c is shown in Fig. A-2. It is supplied to the computer in tabular form as follows:

Displacement (in.)	P_c
0	0
0.10	0.468
0.25	0.502
0.50	0.563
0.75	0.629
1.00	0.697
1.25	0.767
1.50	0.841
1.75	0.920
2.00	1.00
2.49	1.00
2.66	1.823
3.50	1.823
4.50	6.503

Linear interpolation is used between the listed values. The constants and profiles given above apply to each of the three footpads.

III. Body-Block Characteristics

The crush force acting on a crushable body block is given by

$$F_B = A_B C_B P_B (0.75 + 0.25 \cos 2\xi_B)$$

where

F_B = crush force acting normal to the ground surface, lb

A_B = contact area, ft²

C_B = nominal crushing strength per unit area, lb/ft²

P_B = profile to give variation in crushing strength per unit area with displacement, dimensionless

ξ_B = angle of applied load from crushable structure axis, deg

The following numerical values were used in the simulation to describe the body block characteristics:

$$C_B = 5425.6 \text{ lb/ft}^2$$

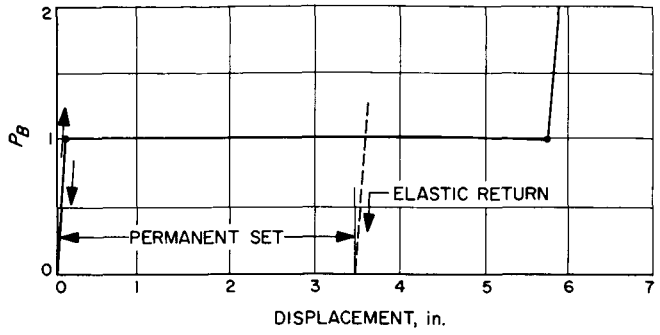

Fig. A-3. Block crush-pressure profile

The profile P_B is shown in Fig. A-3. It is supplied to the computer in tabular form as follows:

Displacement (in.)	P_B
0	0
0.10	1.0
5.75	1.0
7.75	21.0

Linear interpolation is used between the listed values. The constants and profiles given above apply to each of the three body blocks.

Appendix B
Representation of the Coefficient of Sliding Friction in the Computer Program

In the computer simulation, the direction of the friction force acting on any of the spacecraft appendages is such as to oppose the velocity of the appendage.

The coefficient of sliding friction vs sliding velocity as it is treated in the computer program is shown in Fig. B-1, where

μ_0 is the coefficient of sliding friction as specified in the input to the program

$\mu_0 = \mu_B$ for the body blocks

$\mu_0 = \mu_f$ for the footpads

μ is the coefficient of sliding friction used in calculating the friction force.

It is seen from Fig. B-1 that in the computer simulation, as the sliding velocity drops below 1.05 ft/sec, the sliding coefficient of friction is allowed to approach the static coefficient of friction linearly. The static coefficient of friction is assumed to be 20% higher than the sliding coefficient of friction. Below a sliding velocity of 0.05 ft/sec, the coefficient of friction is decreasing from the static coefficient to zero at zero velocity. This is used in the program strictly for computational convenience since the integration routine does not permit the use of step-forcing functions.

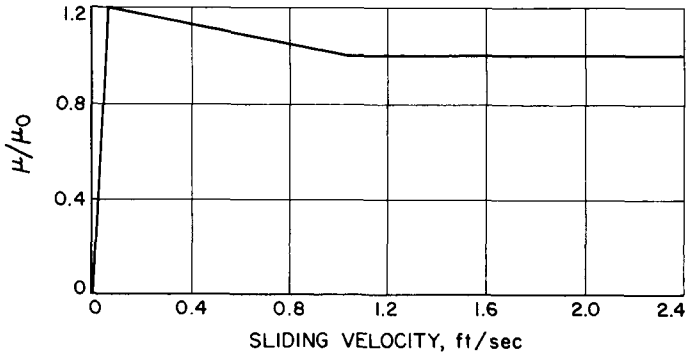

Fig. B-1. Coefficient of sliding friction vs sliding velocity